Ordering Dynamics of Cylindrical and Spherical Microdomains in Polystyrene-*block*-Polyisoprene-*block*-Polystyrene. 1. SAXS and TEM Observations for the Grain Formation

Naoki Sakamoto and Takeji Hashimoto*

Department of Polymer Chemistry, Graduate School of Engineering, Kyoto University, Kyoto 606-8501, Japan

Received March 16, 1998; Revised Manuscript Received October 1, 1998

ABSTRACT: We have investigated the ordering dynamics of a triblock copolymer of a polystyrene-*block*-polyisoprene-*block*-polystyrene with asymmetric composition from the *disordered sphere* phase, where spherical microdomains exist but they have only a short-range liquidlike order, to the cylindrical and spherical microdomains with a long-range order. The ordering process was explored in situ by time-resolved small-angle X-ray scattering (SAXS), and the microdomain structures during the ordering process were observed by transmission electron microscopy (TEM) on specimens frozen at particular times in the ordering process. The SAXS observations show that there is an incubation period before the formation of the cylindrical and spherical microdomains with a long-range order. The coexistence of the ordered grains and the disordered spheres was observed in the TEM pictures taken during the ordering of both cylinders and spheres. The coexistence of the ordered grains and disordered spheres together with the existence of the incubation period suggests that this ordering proceeds via a nucleation and growth process. Moreover, it is revealed that the shape of the ordered grains in the matrix of the disordered spheres highly depends on the microdomain structures.

I. Introduction

Order−disorder transition (ODT) of block copolymer melts has been extensively studied both theoretically and experimentally[1,2] since Leibler's mean-field theory[3] was proposed. Recently, the ordering process of block copolymers has attracted remarkable attention. Fredrickson and Binder[4] proposed the theory concerning the dynamics of the ordering from a disordered state, and many investigators have experimentally studied the ordering dynamics for the block copolymers by means of small-angle X-ray scattering (SAXS),[5−12] small-angle neutron scattering (SANS),[13] low-frequency rheology,[14,15] and depolarized light scattering.[16,17] However, the real-space analysis on the ordering process by using transmission electron microscopy (TEM) has remained unexplored.

Very recently we performed the temperature-drop (*T*-drop) experiments in which the specimens were quenched from the temperatures above the ODT temperature, T_{ODT}, to the temperatures below the T_{ODT} for a nearly symmetric polystyrene-*block*-polyisoprene (SI) diblock copolymer with a lamellar microdomain structure in the ordered state and observed the ordering process after *T* drop by TEM and time-resolved SAXS.[9,11,18] In these studies, the lamellar grains are found to coexist with the disordered phase during the ordering process: the ordered grains grow at the expense of the disordered phase. Moreover, the shape of the lamellar grains in the matrix of the disordered phase is revealed to be highly anisotropic; i.e., their size parallel to lamellar normals is much greater than that perpendicular to them. This feature is consistent with the prediction by Hohenberg and Swift.[19]

In the present study, we conducted the *T*-drop experiments for the polystyrene-*block*-polyisoprene-*block*-polystyrene (SIS) triblock copolymer, Vector 4111, with asymmetric composition and observed the ordering processes of cylindrical and spherical microdomains with TEM and time-resolved SAXS. As shown in Figure 1,[20] this triblock copolymer forms hexagonally packed cylinders at the temperature below the order−order transition (OOT) temperature, T_{OOT}, but spheres with a body-centered-cubic (bcc) lattice above T_{OOT}. With a further increase in the temperature, the bcc lattice is distorted; i.e., the lattice disordering transition (LDT) takes place at the LDT temperature, T_{LDT}. Above T_{LDT}, the spherical microdomains still exist at thermal equilibrium, but they have only a short-range liquidlike order. Hereafter for brevity, we refer to these spherical microdomains with a short-range liquidlike order as "disordered spheres". The true ODT (or microdomain−dissolution transition), where spherical microdomains disappear and transform into thermal concentration fluctuations in a single-phase state, should occur at the ODT temperature (T_{ODT}), higher than T_{LDT}. The precise descriptions for the phase behaviors of Vector 4111 are shown elsewhere[20] and later (see Figure 1). Thus, we can explore the ordering dynamics of hexagonally packed cylinders and that of spheres with a bcc lattice from the disordered spheres for the same block copolymer by quenching Vector 4111 from an initial temperature, T_i ($T_i > T_{LDT}$), to temperatures T_{cyl} ($T_{cyl} < T_{OOT}$) and T_{sph} ($T_{OOT} < T_{sph} < T_{LDT}$), respectively.

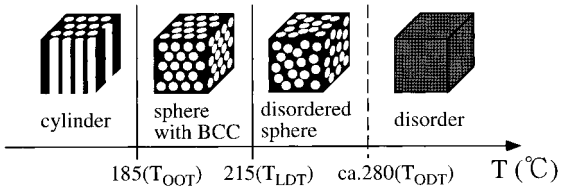

Figure 1. Schematic representation of the microdomain structures for Vector 4111 as a function of temperature.

Because T_{ODT} of Vector 4111 is too high, estimated to be ca. 280 °C,[21] we cannot accomplish a disordered single-phase state for this polymer without thermal

10.1021/ma980411o CCC: $15.00
Published on Web 11/06/1998

degradation and/or cross-linking. Thus, we cannot observe the ordering process of Vector 4111 from the disordered (single phase) melt state. However, the addition of dioctylphthalate (DOP), which is the neutral solvent for polystyrene (PS) and polyisoprene (PI),[22] reduces T_{ODT} to the temperature free from the thermal degradation and/or cross-linking. In our previous paper,[21] the phase behaviors of the solution comprised of 85.5 wt % Vector 4111 and 14.5 wt % DOP (designated as Vector 4111/DOP 85.5/14.5) were found as follows: (1) the system forms hexagonally packed cylinders below 130 °C; (2) the cylinders are transformed into spheres with a bcc lattice at the OOT occurring at 130−135 °C; (3) the bcc spheres persist up to 150 °C; (4) the LDT from spheres with a bcc lattice to the disordered spheres occurs at 150−155 °C and disordered spheres persist up to ca. 205 °C; (5) the ODT occurs at ca. 205 °C, where the disordered spheres continuously transform into thermal concentration fluctuations in the disordered (single-phase) state. To clarify the ordering mechanism of the Vector 4111 solution in DOP from the *disordered single-phase state* and to compare it with the ordering mechanism of Vector 4111 from the *disordered spheres*, we performed the *T*-drop experiment for Vector 4111/DOP 85.5/14.5 from $T_i = 227$ °C ($> T_{ODT}$) to $T_{cyl} = 125$ °C ($< T_{OOT} \ll T_{ODT}$), and the ordering process was explored by time-resolved SAXS.

In the present paper, we shall report the results of the ordering processes of the hexagonally packed cylinders and spheres with a bcc lattice from the *disordered spheres* for Vector 4111 and the ordering process from the *disordered single-phase state* to the hexagonally packed cylinders for Vector 4111/DOP 85.5/14.5.

II. Experimental Method

We employed an SIS triblock copolymer (Vector 4111, Dexco Polymers Co.), which has (i) a weight-average molecular weight of 1.4×10^5, (ii) a volume fraction of PS blocks (f_{PS}) of 0.164, and (iii) a polydispersity index (M_w/M_n) of 1.11. In the present study, we used the as-cast film of Vector 4111, which is prepared as follows: Vector 4111 was first dissolved into toluene to have a 10 wt % solution, and the solvent was evaporated slowly in a fume hood for 1 week and then in a vacuum oven at 170 °C for $^1/_2$ day.

To determine T_{OOT} and T_{LDT}, the static SAXS experiments were conducted under a nitrogen atmosphere, using an apparatus described in detail elsewhere.[23−25] The SAXS apparatus consists of an 18-kW rotating-anode X-ray generator (MAC Science, Yokohama, Japan), a graphite crystal for incident-beam monochromatization, a 1.5-m camera, and a one-dimensional position-sensitive proportional counter (1D-PSPC). The Cu Kα line ($\lambda = 0.154$ nm) was used. The SAXS profiles were measured in situ as a function of temperature in the heating and cooling processes. At each temperature, the specimens were held for 10 min before the measurement and then the measurement lasted at this temperature for 50 min in the heating process. In the cooling process, the specimens were held at each temperature for 15 min before measurement and then the measurement lasted for 30 min.

The ordering processes of hexagonally packed cylinders and spheres with a bcc lattice from disordered spheres were explored by the *T*-drop experiments in which the specimens were quenched from $T_i = 237$ °C ($T_i > T_{LDT}$) to $T_{cyl} = 175$ °C ($T_{cyl} < T_{OOT}$) and $T_{sph} = 197$ °C ($T_{OOT} < T_{sph} < T_{LDT}$), respectively. The ordering processes after *T* drop were observed by time-resolved SAXS and TEM. The quenching process was done as follows: first the specimen placed in the sample cell[26] was put in a heater block which was set on the optical path of an incident X-ray beam and regulated at T_i and then the temperature of the heater block was rapidly changed into T_{cyl} or T_{sph}. The time-resolved SAXS measurements were started and set to zero when the temperature reached the measuring temperature. The temperature in the specimen reaches the measuring temperature within ca. 2 min after *T* drop.

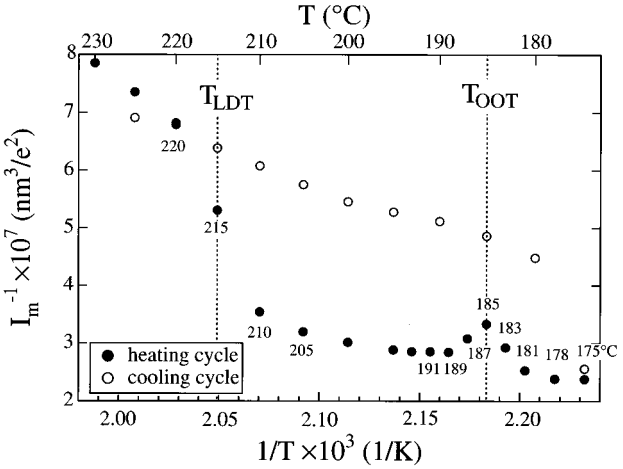

Figure 2. I_m^{-1}, obtained in the heating and cooling processes, plotted as a function of $1/T$ for Vector 4111.

The SAXS profiles obtained were corrected for absorption, air scattering, and background scattering arising from thermal diffuse scattering and slit-height and slit-width smearing.[23−25] The absolute SAXS intensity was obtained using the nickel-foil method.[27]

The structures during the ordering were observed by TEM. At a given time after *T* drop from T_i to T_{sph} or T_{cyl} with the same method as that used in the time-resolved SAXS experiments, the specimen was put into an ice−water bath at 0 °C. Because the glass transition temperature (T_g) of the PS component in the block copolymer is higher than 0 °C, we could freeze the structure at the moment when the system was put into the ice−water.[18] Thus, we could investigate the structures frozen during the ordering with TEM. The frozen specimens at 0 °C were subjected to microtoming into the ultrathin sections of ca. 50-nm thickness at −85 °C with a Reichert-Jung ultracut E together with a cryogenic unit FC 4E and a glass knife. The ultrathin sections were quickly picked up on 400-mesh copper grids and stained by osmium tetroxide vapor at room temperature for about $^1/_2$ day. TEM observation was made with a Hitachi H-600 transmission microscope at 100 kV.

The ordering process of the Vector 4111/DOP 85.5/14.5 from the disordered single-phase state to the hexagonally packed cylinders was observed by time-resolved SAXS by quenching the specimen from $T_i = 227$ °C to $T_{cyl} = 125$ °C with the same method as described above.

III. Experimental Results

III-1. Phase Behaviors of Vector 4111. To determine T_{OOT} and T_{LDT} of Vector 4111, the static SAXS experiments were conducted. Because the scattering behaviors of Vector 4111 were described precisely in the previous paper,[20] here we shall briefly summarize the SAXS results. Figure 2 gives the reciprocal of the scattered intensity, I_m^{-1}, at the first-order SAXS maximum, plotted as a function of the reciprocal of the absolute temperature, $1/T$.[20] In the heating process, I_m^{-1} changes between 183 and 189 °C. This indicates that the OOT from hexagonally packed cylinders to spheres with a bcc lattice starts at 183 °C and ends at 189 °C. Furthermore, I_m^{-1} increases discontinuously at around 210 °C, indicating that the LDT from spheres with a bcc lattice to the disordered sphere starts at ca. 210 °C.

In the cooling process, there is no discontinuity in I_m^{-1} from 220 to 180 °C, indicating that the system stays in

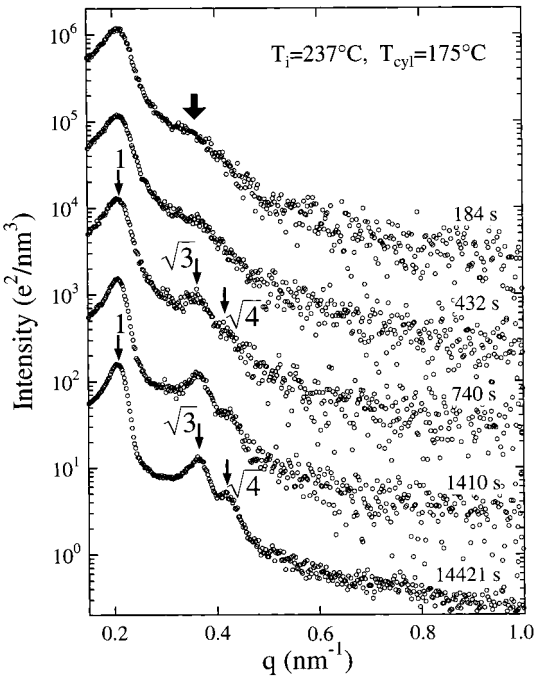

Figure 3. Time evolution of the SAXS profiles for Vector 4111 after T drop from T_i = 237 °C to T_{cyl} = 175 °C (see Figure 1). To prevent any artifacts induced by the slit corrections, the profiles without slit corrections are shown here.

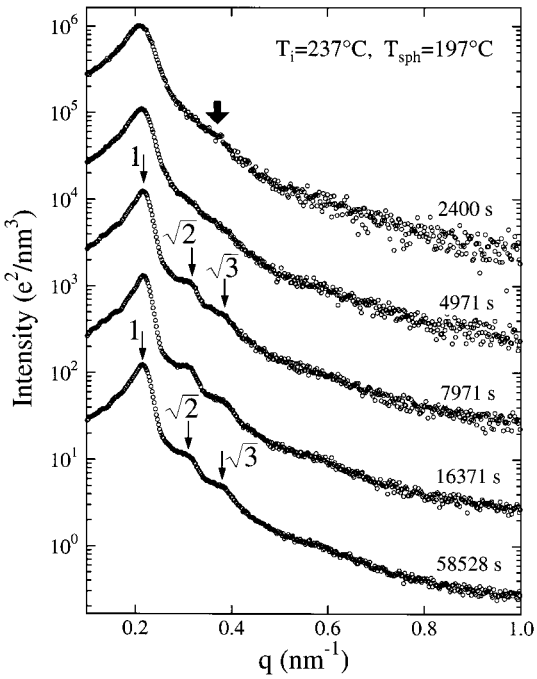

Figure 4. Time evolution of the SAXS profiles for Vector 4111 after T drop from T_i = 237 °C to T_{sph} = 197 °C (see Figure 1). To prevent any artifacts induced by the slit corrections, the profiles without slit corrections are shown here.

the disordered spheres down to 180 °C. The transition from disordered spheres to hexagonally packed cylinders takes place at 175 °C. Here it should be mentioned that the disordered spheres at temperatures between 210 and 180 °C were not equilibrium. Because it takes a very long time for the disordered spheres to be transformed into the spheres with a bcc lattice, the system remains in the **supercooled disordered sphere state** down to 180 °C within the time scale of this experiment. The ordering from disordered spheres to hexagonally packed cylinders is faster than that to bcc spheres.[28] Hence, the ordering to hexagonally packed cylinders at 175 °C occurs within the time scale of this experiment.

The phase behavior of Vector 4111 thus obtained is schematically illustrated in Figure 1. T_{ODT} was estimated to be ca. 280 °C from T_{ODT} of Vector 4111/DOP 85.5/14.5 by assuming $T_{ODT,b} = T_{ODT,s}/\phi_p$,[28-31] where $T_{ODT,b}$, $T_{ODT,s}$, and ϕ_p are T_{ODT}'s for the neat Vector 4111 and Vector 4111 solution in DOP and the volume fraction of Vector 4111 in the solution, respectively.[21]

In the present study, T_{OOT} and T_{LDT} are slightly different from those obtained in the previous study (T_{OOT} = 179−185 °C and T_{LDT} = 210−214 °C in the previous study[20]), as a consequence of repreparation for the solvent-cast film of the specimens, though the difference is very small. This difference may be due to the small amount of the thermal degradation or cross-linking reaction in either or both specimens used in the present or previous study.

III-2. *T*-Drop Measurements for the Neat Vector 4111. (1) SAXS Observations. Figure 3 shows the time evolution of the SAXS profiles after T drop from T_i = 237 °C to T_{cyl} = 175 °C, plotted as a function of the scattering vector q. The quantity q is defined by

$$q = (4\pi/\lambda)\sin(\theta/2) \quad (1)$$

where λ and θ are the wavelength and scattering angle in the medium, respectively. The intensities of the profile shown at the top of this figure are actual values, and to avoid overlaps, the intensities of other profiles were shifted down by 1 decade relative to the intensities immediately above. The SAXS profiles shown later (in Figures 4, 13a, and 14) will be also presented in the same manner as that in Figure 3. To prevent any artifacts that might be induced by the slit corrections, Figure 3 shows the profiles without the slit corrections. It is worth noting in Figure 3 that the profiles at 184 and 432 s have a broad first-order peak and a second-order shoulder at q = 0.35 nm^{-1}, with the latter being marked by a thick arrow. The second-order shoulder indicates that there are spheres with a short-range liquidlike order as predicted by Percus−Yevick theory[32] or by a paracrystal model with a very large distortion.[33] At 740 s, the first-order peak becomes sharp discontinuously (as will be demonstrated later in Figure 5) and the distinct higher-order peaks appear at $q = \sqrt{3}q_m$ and $\sqrt{4}q_m$, where q_m is the wave vector at the first-order peak, indicating that the hexagonally packed cylinders are formed. The first-order and higher-order peaks of the profiles get sharper with increasing time after 740 s.

Figure 4 gives the time evolution of the SAXS profiles after T drop from T_i = 237 °C to T_{sph} = 197 °C. To prevent any artifacts induced by the slit corrections, Figure 4 shows the profiles without the slit corrections. It is worth noting in Figure 4 that the profile at 2400 s has a broad first-order peak and a second-order shoulder at q = 0.35 nm^{-1}, with the latter being marked by a thick arrow. At 7971 s, the first-order peak becomes sharp discontinuously (as will be demonstrated in Figure 5) and the distinct higher-order peaks appear at $q = \sqrt{2}q_m$ and $\sqrt{3}q_m$, indicating that spherical microdomains with a cubic lattice exist. The first-order and higher-order peaks of the profiles get sharper with increasing time after 7971 s.

The cubic lattice of the spherical microdomains may be either bcc or sc (simple cubic). However, because the

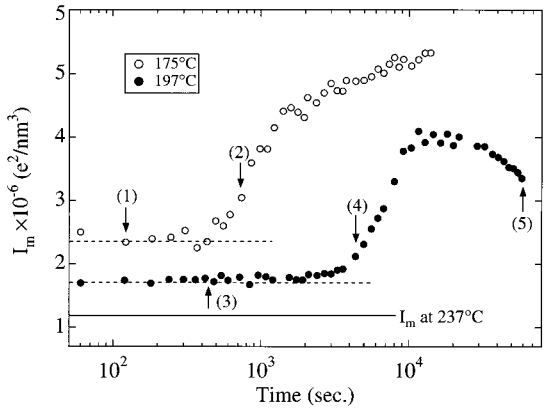

Figure 5. Time evolution of I_m for Vector 4111 after T drop from T_i = 237 °C ($> T_{LDT}$) to 175 and 197 °C ($< T_{LDT}$). The arrows show the time when the TEM observations were made. The horizontal solid line shows the equilibrium value at the initial temperature T_i = 237 °C, and the broken lines show the values for the supercooled disordered spheres at 197 and 175 °C obtained or estimated from the static SAXS experiment in the cooling process (see Figure 2).

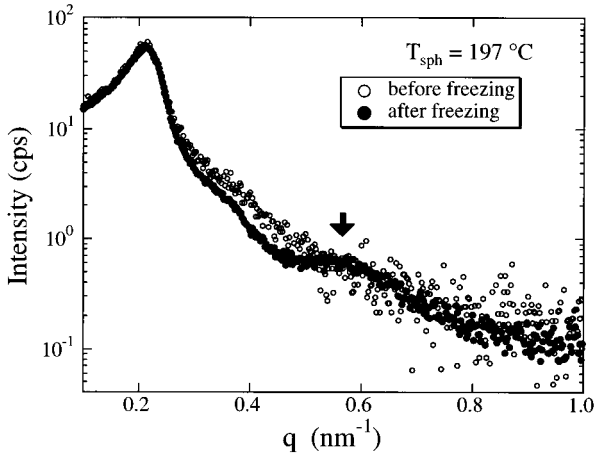

Figure 6. Comparison of the SAXS profiles measured before (○) and after (●) freezing at 432 s after T drop to T_{sph} = 197 °C.

differentiation between the two symmetry groups from the positions of scattering maxima requires seven diffraction maxima,[34] we cannot distinguish bcc and sc. Therefore, we use another method given below for the differentiation. In the SAXS profile at 58 528 s, a weak peak corresponding to the form factor of spherical domains is observed around $q = 0.55$ nm^{-1}. Although this peak is not clear in this figure, we observed the more obvious peak in the SAXS profile obtained from the specimens quenched into an ice−water bath after the ordering for 58 528 s. This trend is the same as that observed in Figure 6 described below. Thus, the peak position of the scattering from the form factor of spherical domains and q_m enable us to determine the radius of the spherical particles, R, and the domain spacing, D, as 10.5 and 28.6 nm, respectively.[35] Here it should be noted that we used the scattering profile with slit corrections to obtain these values. When the values of D and R are used, the volume fractions of spherical microdomains with sc and bcc lattices can be calculated.[35] The volume fractions of spherical microdomains thus obtained are 0.207 and 0.146 for sc and bcc lattices, respectively. It should be noted that f_{PS} of Vector 4111 corresponding to the volume fraction of polystyrene microdomains is 0.164, which is close to the value of 0.146 for a bcc lattice. Thus, we can conclude that the spherical microdomains at 197 °C have a bcc lattice.

Figure 5 gives the time evolution of the peak intensity, I_m, after T drop to T_{cyl} = 175 and T_{sph} = 197 °C. The values of I_m were obtained from the SAXS profiles corrected for the slit smearings. The horizontal solid and broken lines show the equilibrium value at T_i = 237 °C and the values for the supercooled disordered spheres at 197 and 175 °C obtained or estimated from the static SAXS experiment in the cooling process (see Figure 2), respectively.

The arrows indicate the time when the TEM observations were done. It is found in Figure 5 that in both cases, at 175 and 197 °C, the values of I_m change from the equilibrium value at 237 °C to the values of 2.3 × 10^6 and 1.8 × 10^6 e^2/nm^3, respectively, within the shortest time covered in these experiments, and then I_m stays there for a certain incubation period. After this period, I_m at 175 and 197 °C starts to increase at ca. 500 and 6000 s, respectively. The incubation period in the ordering of hexagonally packed cylinders[12] and spheres[10] with a bcc lattice from the disordered state was reported previously.

(2) TEM Observations. 2-a. Structure in the Incubation Period for the Ordering. TEM observations were performed for the specimens frozen with ice−water at a particular time during the ordering and then stained with OsO_4. To check whether the freezing process changed the structure in the system, the profiles measured before and after freezing at 432 s after T drop to 197 °C are compared in Figure 6. The profile after freezing (filled circles) is slightly different from that before freezing (open circles): the profile after freezing shows an obvious scattering maximum at $q = 0.55$ nm^{-1} (marked by a thick arrow), but that before freezing does not. However, this scattering maximum at 0.55 nm^{-1} corresponds to the maximum of the particle scattering from the spheres, which relates to R, the distribution of R, the sharpness of the interface, and the electron density difference between PS spheres and the PI matrix. On the other hand, the sharpness of the first-order peak corresponding mainly to a spatial distribution of the spheres does not change in the freezing process. Thus, it is confirmed that the freezing process did not change the spatial distribution of spheres related to a long-range order. Using the method as described above, we confirmed in every case of freezing that the freezing-in process does not change the long-range order of the particles.

Figure 7 gives the TEM picture for the specimen frozen at 432 s after T drop to T_{sph} = 197 °C. The state at 432 s is shown by arrow 3 in Figure 5 (the state in the incubation period). It is noted that the microdomain structure in Figure 7 is very similar to that presented in Figure 1c in ref 20, which shows the disordered spheres for Vector 4111 at 200 °C, which is above T_{LDT} but below T_{ODT}. The microdomain structure appears to be composed of small bright (PS) spheres with diameter of ca. 25 nm and a dark (PI) matrix with only a short-range order, though some of the bright domains, such as the one in the white circle in the inset, are highly distorted.

Figure 8 gives the TEM picture for the specimen frozen at 122 s after T drop to T_{cyl} = 175 °C. The state at 122 s is shown by arrow 1 in Figure 5 (the state in the incubation period). It is noted that the microdomain

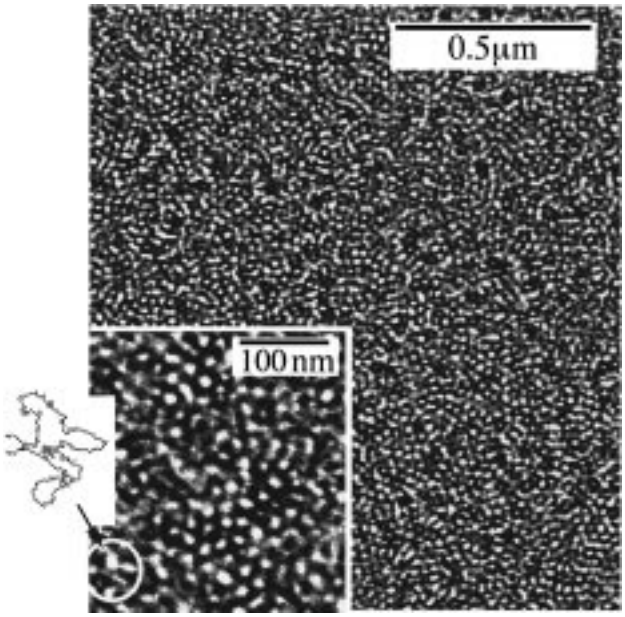

Figure 7. Transmission electron micrograph for Vector 4111 frozen at 432 s after *T* drop to 197 °C. The inset shows a magnified micrograph. The sketch drawn in the left margin of the inset shows the outline of the distorted bright domain in the white circle.

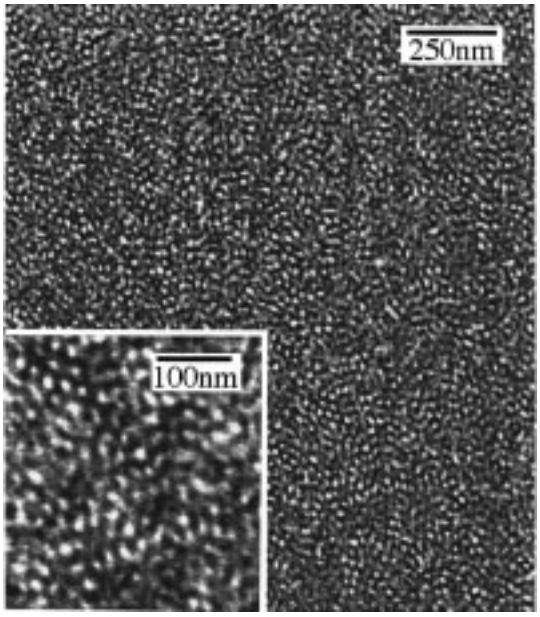

Figure 8. Transmission electron micrograph for Vector 4111 frozen at 122 s after *T* drop to 175 °C. The inset shows a magnified micrograph.

structure in Figure 8 is very similar to that presented in Figure 7, indicating that the disordered spheres are formed in the incubation period even at 175 °C.

2-b. Structure during the Formation of Cylindrical Microdomains. Figure 9 gives the TEM picture for the specimen frozen at 740 s after *T* drop to T_{cyl} = 175 °C. The state at 740 s is shown by arrow 2 in Figure 5. It is noted in Figure 9 that the many ordered grains are observed in the matrix of the less ordered phase. The less ordered matrix (inset a) is similar to the structure observed in Figure 7. In Figure 9, some ordered grains seem to be composed of a hexagonally packed bright spot in the matrix of the dark phase as seen in inset b and other ones seem to be composed of the alternative dark and bright stripes as seen in inset

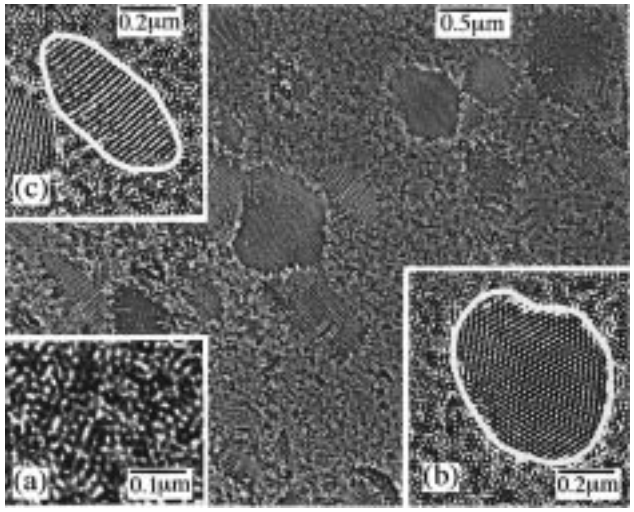

Figure 9. Transmission electron micrograph for Vector 4111 taken at 740 s after *T* drop to 175 °C. Insets a−c highlight the less ordered matrix and the ordered grains in which the cylindrical axis aligns perpendicular and parallel to the ultrathin section of the specimen, respectively. The outline of the ordered grains in insets b and c is traced by the white lines.

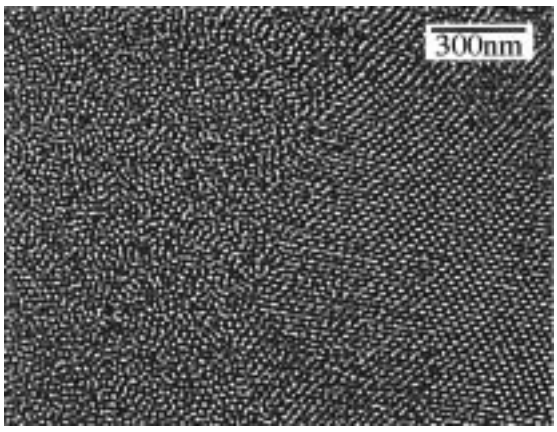

Figure 10. Transmission electron micrograph for Vector 4111 which highlights the grain boundary, running vertically in the center, between the ordered grain and disordered spheres for the specimen frozen at 4873 s after *T* drop to 197 °C.

c, indicating that the ordered grains in Figure 9 are composed of hexagonally packed PS cylinders in the PI matrix. It should be mentioned that the shape of the ordered grains in which the cylindrical axis aligns perpendicular to the ultrathin section of this specimen is almost isotropic, as shown in inset b, but that of the ordered grains in which the cylindrical axis aligns parallel to the ultrathin section are anisotropic, as shown in inset c: the size along the cylindrical axis is much smaller than that perpendicular to it.

2-c. Structure during the Ordering into bcc Spheres. The TEM pictures for Vector 4111 frozen at 4873 s after *T* drop to T_{sph} = 197 °C are given in Figure 10, which highlight the boundary between the ordered grain and less ordered phase, and in Figure 11, which highlights the whole image of the ordered grain embedded in the less ordered phase. The state at 4873 s is shown by arrow 4 in Figure 5. It is noted that the bright (PS) spherical particles on the right-hand side in Figure 10 align with regularity, while the PS particles on the left-hand side align randomly, indicating that the ordered grain composed of spherical microdomains with a long-range order coexists with the less ordered phase

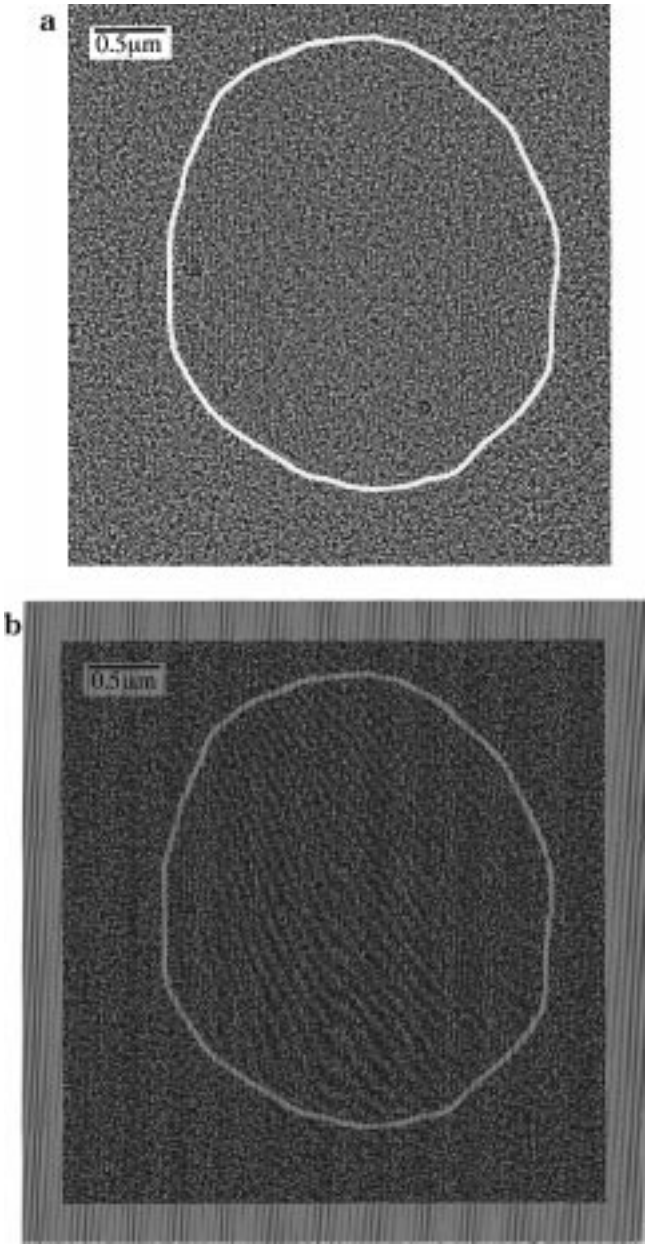

Figure 11. Transmission electron micrographs for Vector 4111 which highlights a whole image of the ordered grain for the specimen frozen at 4873 s after T drop to 197 °C. Parts a and b show just the same image. The white lines drawn in the micrographs of parts a and b show the outline of the ordered grain. In part b, to demonstrate the shape of the ordered grain more clearly, the artificial stripes with a spacing corresponding to 25 nm are overlaid. The moiré fringes observed inside the white circle drawn in the center of part b indicate that a spherical ordered grain with a bcc lattice exists.

of the spherical domains (disordered spheres) in this picture.

To show a whole shape of the ordered grain, Figure 11a gives a lower magnification picture than that in Figure 10. However, the magnification in Figure 11a is too low to distinguish the ordered grain, which exists inside a white circle marked on the micrograph, from the less ordered microdomains. To clarify the grain boundary between the ordered grain and less ordered phase more clearly than in Figure 11a, in Figure 11b the artificial stripes with the spacing corresponding to 25 nm are overlaid in Figure 11a. In Figure 11b the moiré fringes are seen in the center of this picture with

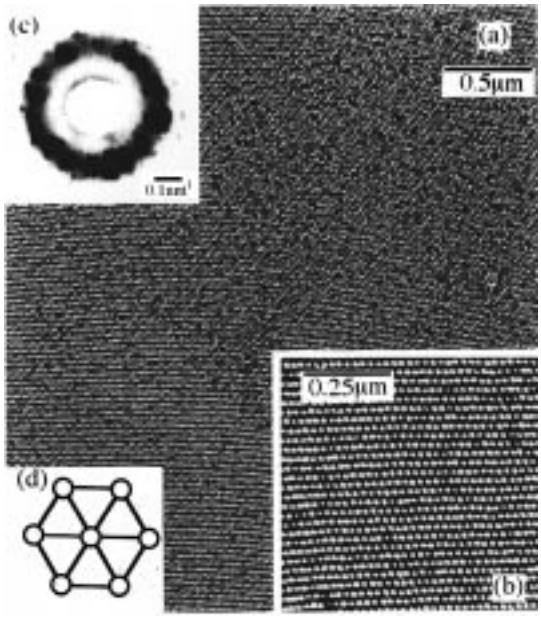

Figure 12. (a) Transmission electron micrograph for Vector 4111 frozen at 67 000 s after T drop to 197 °C. Inset b shows a magnified micrograph. Inset c shows the 2D SAXS pattern obtained in situ at 41 400 s after T drop to 205 °C. Inset d shows the [111] projection of a bcc lattice.

the spacing of ca. 0.1 μm, indicating that there is an ordered grain in which the spherical microdomains align with a long-range order and the direction of the alignment is slightly different from that of the stripes. Thus, we could determine the shape of the ordered grain. The outline of the ordered grain obtained is traced by a white line in Figure 11. The ordered grain has the almost isotropic shape and the size of ca. 3 μm. Here it should be mentioned that the ordered grain in Figure 11 is one of the smallest ordered grains found in this experiment. Most of the grains found in this experiment are larger than 3 μm.

Figure 12 gives the TEM picture for the specimen frozen at 67 000 s after T drop to T_{sph} = 197 °C. The state at 67 000 s is shown by arrow 5 in Figure 5. It is noted in Figure 12 that the spherical microdomains with a long-range order fill all of the space. The micrograph shows [111] projection of bcc spheres, as highlighted in the enlarged micrograph (inset b) and as shown by the inset d. The ordering from disordered spheres to spheres with a long-range order has finished. Furthermore, no grain boundary is observed in Figure 12, indicating that the spherical microdomains form a large grain, the size of which is more than 3 μm at least.

For the specimen at 41 400 s after T drop to T_{sph} = 205 °C, the SAXS experiment with the imaging plate (IP)[36] as the two-dimensional (2D) detector was performed. In this measurement, the incident beam was collimated with two pinholes of 0.5-mm ϕ set at a distance of 30 cm apart in front of the specimen. The sample thickness was ca. 2 mm. Because the ordering process at 205 °C is almost identical to that at 197 °C, the structure at 41 400 s after T drop to 205 °C can be considered to be the same as that at 67 000 s after T drop to 197 °C. The 2D SAXS pattern thus obtained is given in Figure 12c. This pattern shows a number of discrete diffraction spots rather than a continuous ring, indicating that the grain size in the specimen is considerably large.[37] The precise description about this experiment with the IP will be presented elsewhere.[28]

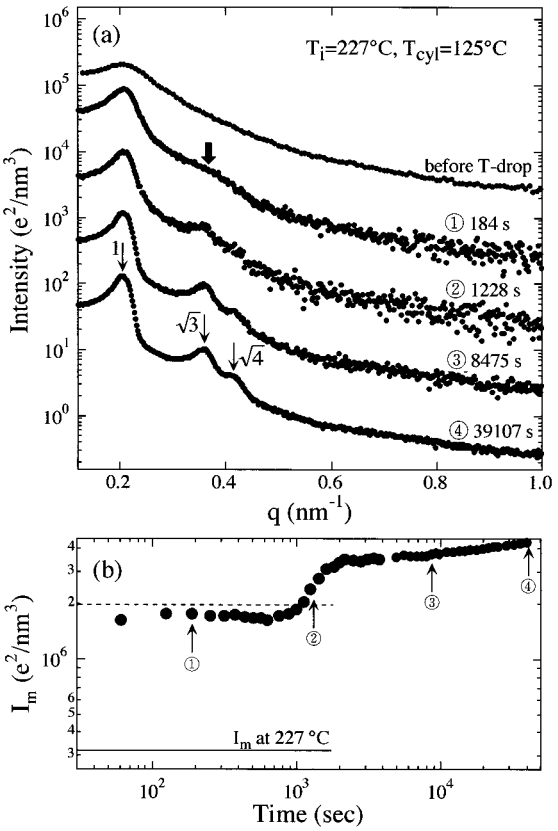

Figure 13. Time evolution of (a) the SAXS profiles and (b) I_m for Vector 4111/DOP 85.5/14.5 after T drop from $T_i = 227$ °C ($> T_{ODT}$) to $T_{cyl} = 125$ °C ($< T_{OOT} \ll T_{ODT}$). The SAXS profile before T drop is also presented in part a for reference. To prevent any artifacts induced by the slit corrections, the profiles without slit corrections are shown in part a. The horizontal solid and broken lines in part b show, respectively, the equilibrium value at the initial temperature 227 °C and the values for the supercooled disordered spheres at 125 °C estimated from the static SAXS experiment for Vector 4111/DOP 85.5/14.5 in the cooling process.[21] The numbers in part b correspond to those attached to the scattering profiles in part a.

III-3. *T*-Drop Measurement for Vector 4111/DOP 85.5/14.5. To compare the ordering process from the disordered spheres with that from the disordered single-phase state, we performed the T-drop experiment for Vector 4111/DOP 85.5/14.5 from $T_i = 227$ °C ($> T_{ODT}$) to $T_{cyl} = 125$ °C ($< T_{OOT} \ll T_{ODT}$).

Figure 13 gives the time evolution of the SAXS profiles (part a) and I_m (part b) after T drop to 125 °C. The values of I_m in part b were obtained from the SAXS profiles corrected for the slit smearings, but the SAXS profiles in part a were not corrected for the slit smearings in order to prevent any artifacts induced by the slit corrections. The horizontal solid and broken lines in part b show, respectively, the equilibrium value at the initial temperature 227 °C, and the value for the supercooled disordered spheres at 125 °C estimated from the static SAXS experiment for Vector 4111/DOP 85.5/14.5 in the cooling process.[21]

The profile before T drop has only one broad peak and no higher-order peaks or shoulder, but that at 184 s has a second-order shoulder at $q = 0.35$ nm^{-1}, as shown by a thick arrow, suggesting that the system changes from the disordered single-phase state to the disordered spheres within 184 s after T drop, as will be discussed in detail in section IV. At 8475 s, the first-order peak becomes sharp and the distinct higher-order peaks can be observed at $q = \sqrt{3}q_m$ and $\sqrt{4}q_m$, indicating that the hexagonally packed cylinders appear from the disordered spheres. In Figure 13b, the I_m changes from the value at the initial state to 1.6×10^6 e^2/nm^3 within 60 s. The system changes from the disordered state to the disordered spheres within 60 s after T drop. The following process is similar to the ordering in Figure 5.

IV. Discussion

IV-1. Ordering Processes of Hexagonally Packed Cylinders and Spheres with a bcc Lattice from Disordered Spheres. In Figure 5, the time evolution of I_m at 175 and 197 °C shows similar trends: (1) after T drop to 175 and 197 °C, the values of I_m change from the equilibrium value at $T_i = 237$ °C to 2.3×10^6 and 1.8×10^6 e^2/nm^3, respectively, within the shortest time covered in this experiment; (2) I_m stays there for a certain period; (3) after this incubation period, I_m at 175 and 197 °C starts to increase at 500 and 6000 s, respectively. The existence of the incubation period suggests that the ordering proceeds via a nucleation and growth process.

The value of I_m^{-1} for the supercooled disordered spheres at 197 °C obtained from the static SAXS experiment in the cooling process is ca. 5.5×10^{-7} nm^3/e^2, and that at 175 °C estimated from the extrapolation of the static SAXS data above 180 °C obtained in the cooling process is ca. 4.5×10^{-7} nm^3/e^2 (see Figure 2). The corresponding values of I_m are ca. 1.8×10^6 and 2.2×10^6 e^2/nm^3, respectively. These values are very close to I_m in the incubation period after T drop to 197 °C (1.8×10^6 e^2/nm^3) and 175 °C (2.3×10^6 e^2/nm^3). Moreover, the SAXS profiles in this time period show the broad second-order shoulder as shown in Figures 3 and 4, indicating that there are spheres with the short-range liquidlike order as discussed in section III-2-a. These evidences indicate that the system forms the supercooled disordered spheres in the incubation period. This is valid even at 175 °C, where the hexagonal cylinders are eventually formed.

Figures 7 and 8 show the TEM picture taken in the incubation period after T drop to 197 and 175 °C, respectively. The microdomains are composed of small bright (PS) particles with diameter of ca. 25 nm and a dark (PI) matrix, though some of them form distorted domains such as the one marked by an arrow in the inset of Figure 7. We interpret this distortion as a result of an overlap of the spherical particles in the depth direction. This is because the diameter of spheres is ca. 25 nm and the thickness of the ultrathin section of the specimen for TEM is ca. 50 nm; thus, spherical particles can be overlapped in the depth direction, giving rise to the appearance of the distorted domains, when the system lacks a bcc symmetry. Thus, the TEM picture also reveals that the system forms the supercooled disordered spheres of PS in the incubation period.

Figure 8 shows essentially the same morphology as that found in Figure 7. Here it should be mentioned that the morphology in the equilibrium state at 175 °C is hexagonally packed cylinders. Nevertheless, to our surprise, the structure in the incubation period at 175 °C is also comprised of the disordered spheres: the hexagonally packed cylinders is transformed from disordered spheres but not from disordered cylinders.

In Figures 9−11, the ordered grains and the less ordered phase coexist in the ordering process. The less ordered phase is similar to the structure in Figures 7

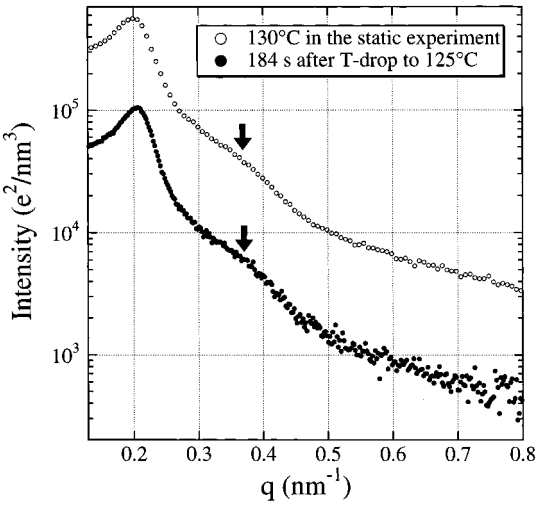

Figure 14. Comparison of the SAXS profiles measured at 130 °C (○) in the static SAXS experiment for Vector 4111/DOP 85.5/14.5 in the cooling process[21] and at 184 s (●) after quenching Vector 4111/DOP 85.5/14.5 from 227 to 125 °C.

and 8, indicating that the less ordered phase in Figures 9−11 is composed of the disordered spheres. Note again that the equilibrium morphology of the ordered grains in Figure 9 is hexagonally packed cylinders. The ordered cylinders do not coexist with the disordered cylinders, but they do coexist with the disordered spheres. The coexistence of the ordered grains and disordered spheres supports that this ordering proceeded by a nucleation and growth process: the ordered grains grow at the expense of the disordered sphere phase.

The ordering process studied by using the neat Vector 4111 is the ordering from disordered spheres but not from a disordered single phase. The latter is clearly demonstrated from the SAXS results shown in Figure 13: the ordering process from the disordered single-phase state to the hexagonally packed cylinders is shown for Vector 4111/DOP 85.5/14.5. In this case, the SAXS profile changes very rapidly from the initial one in the disordered single-phase state to the one in the incubation period. To elucidate the state in the incubation period, in Figure 14 the SAXS profile in the incubation period [point 1 in Figure 13b] is compared with the profile obtained at 130 °C in the static SAXS experiment for Vector 4111/DOP 85.5/14.5 in the cooling process.[21]

In the previous study, we found that, in the cooling process from 220 °C ($> T_{ODT}$), the disordered spheres are stable down to 130 °C, though bcc spheres are observed at temperatures between 135 and 150 °C in the heating process.[21] Thus, the SAXS profile at 130 °C in Figure 14 corresponds to the scattering from the supercooled disordered spheres of Vector 4111/DOP 85.5/14.5. In Figure 14, the SAXS profile in the incubation period at 184 s after T drop to 125 °C is very similar to that at 130 °C: both profiles have a broad second-order shoulder as shown by thick arrows, though the peak at 184 s is slightly sharper than that at 130 °C, because the temperature (125 °C) employed in the T-drop measurement is lower than 130 °C. Furthermore, in Figure 13b I_m in the incubation period is very close to the value at 125 °C estimated from the static SAXS experiment for Vector 4111/DOP 85.5/14.5 in the cooling cycle. Thus, it can be concluded that the system forms the supercooled disordered spheres in the incubation period.

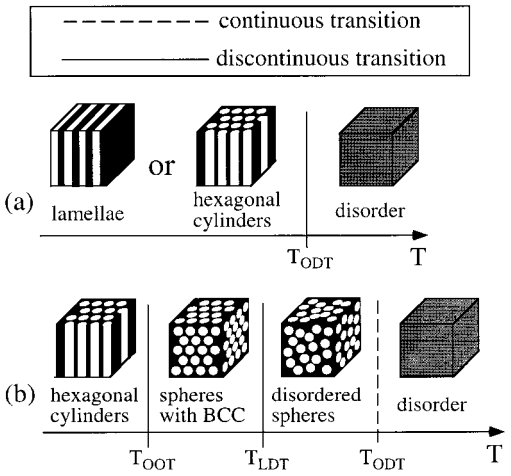

Figure 15. Schematic representation of the phase behaviors for (a) the block copolymers employed in the previous studies[7−9,11−18] and (b) the neat Vector 4111 and Vector 4111/DOP 85.5/14.5.

The ordering process after the system reaches the disordered spheres is very similar to the ordering from the disordered spheres in the neat Vector 4111. Thus, we can conclude that, after T drop from the disordered single-phase state, the system changes very rapidly into the disordered spheres, and the following ordering process is identical with that directly from the disordered spheres.

Here it should be mentioned that in previous reports[7−9,11−18] the ordered grains of lamellar and cylindrical microdomains appear directly from the disordered single-phase state in the ordering process of the block copolymers, in contrast to the case of Vector 4111/DOP 85.5/14.5. This difference may be related to the phase behaviors of the block copolymers, as schematically shown in Figure 15. The block copolymers employed in the previous studies show the discontinuous ODT: upon increasing temperature through T_{ODT} the ordered microdomains with a long-range order are directly transformed into the fluctuation-induced single-phase disorder state (part a), while Vector 4111 and Vector 4111/DOP 85.5/14.5 undergo the discontinuous LDT before they reach the apparently continuous ODT (part b). In case b, the ordering of the block copolymers from the disordered single phase into the bcc spheres was elucidated to proceed via the formation of the disordered sphere phase. Moreover, when the specimen is quenched into the temperature below T_{OOT}, cylindrical microdomains develop from the disordered spheres.

According to our previous report,[18] the ordering of the nearly symmetric SI diblock copolymer after T drop from a disordered state to an ordered state proceeds by nucleation and growth via the following three stages: (1) the thermal concentration fluctuations relax rapidly from the initial state before T drop to the disordered state at a temperature very close to T_{ODT} within the shortest time covered in the experiment; (2) the system stays at that state for a certain incubation period; (3) the formation of the lamellar structure starts after this incubation period. These ordering processes are very similar to that in this experiment, except for the state in the incubation period: the disordered single phase for a symmetric SI diblock copolymer versus the disordered spheres in the present study.

IV-2. Shape of the Ordered Grains Composed of Various Microdomain Structures in the Matrix of the Less Ordered Phase. In Figure 9, the shape

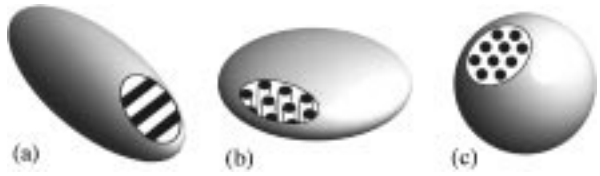

Figure 16. Schematic representation of the ordered grains composed of (a) lamellar, (b) cylindrical, and (c) spherical microdomain structures in the matrix of the less ordered phase.

of the ordered grains in which the cylindrical axis aligns perpendicular to the ultrathin section of the specimen is almost isotropic, but that of the ordered grains in which the cylindrical axis aligns parallel to the ultrathin section of the specimen is anisotropic, revealing that the grain size along the cylindrical axis is much smaller than that perpendicular to it; i.e., the ordered grains in the matrix of the disordered spheres form a lenslike oblate ellipsoidal grain, where the cylinders are packed parallel to the short axis of the oblate ellipsoid, as shown schematically in Figure 16b.

On the other hand, the shape of the ordered grain with the spheres in a bcc lattice is almost isotropic as shown in Figure 11, indicating that the spherical microdomains with a bcc lattice form nearly spherical grains, as shown schematically in Figure 16c. Previously, we reported that the ordered lamellar grains in the matrix of the disordered phase are highly elongated toward the direction parallel to lamellar normal; i.e., the lamellar grains form a cigarlike prolate ellipsoidal grain, as shown schematically in Figure 16a.[11,18] Thus, we can summarize the shape of the ordered grains composed of various microdomain structures in the matrix of the less ordered phase, as shown schematically in Figure 16.

Recently, Hohenberg and Swift[19] estimated the anisotropic interfacial free energy, $\sigma_\perp$ and $\sigma_\parallel$, on the interface between the ordered grain of lamellae and the matrix of the disordered phase (referred to as the **grain interface** hereafter) for the lamellar grains isolated in the disordered phase and concluded $\sigma_\perp < \sigma_\parallel$ near the ODT, where $\sigma_\perp$ and $\sigma_\parallel$ are the interfacial free energies on the transverse and longitudinal grain interfaces perpendicular and parallel to the lamellar interfaces, respectively. In this case, the shape of the nucleated lamellar grains is predicted to be anisotropic: the grains are elongated parallel to the lamellar normal. This prediction is consistent with the result shown in Figure 16a.

Unfortunately, the shape of the ordered grains composed of the cylindrical or spherical microdomains in the matrix of the disordered spheres has not been theoretically estimated so far. The lenslike grains composed of the cylindrical microdomains were reported also by Koizumi et al.[38] for a mixture of the SI diblock copolymer, forming hexagonally packed cylindrical microdomains in the equilibrium, and homopolymer (HS). The mixture underwent macrophase separation between SI and HS and formed the grains composed of the hexagonally packed cylinders in the HS matrix. The observed lenslike grains were interpreted on the basis of anisotropic interfacial tension between the grains and the matrix. We may apply essentially the same argument in our system:[39] the lenslike grains result from the difference of the interfacial tension at the macroscopic interface between the grain and the matrix; i.e., the interfacial tension $\sigma_\perp$ of the transverse grain interfaces which are normal to the cylinder axis is smaller than the interfacial tension $\sigma_\parallel$ of the longitudinal grain interfaces which are parallel to the cylinder axis.

Very recently Dai et al.[17] performed the *T*-drop experiment from the disordered state to the ordered state for the SI diblock copolymer and observed the ordering process of cylindrical microdomains by depolarized light scattering. They reported that the ordered grains composed of the cylinders, appearing from the disordered phase after *T* drop, are highly anisotropic: the size along the optical axis is *larger* than that perpendicular to it. Here it should be noted that the optical axis of cylindrical microdomains is parallel to the cylindrical axis, because the anisotropy primarily arises from the form anisotropy.[40] Therefore, their results mean that the size along the cylindrical axis is much *larger* than that perpendicular to it, a trend of which is opposite to our results.

V. Concluding Remarks

We studied the ordering process for the triblock copolymer, Vector 4111, with asymmetric composition by means of time-resolved SAXS and TEM. The time evolution of I_m indicates that the ordering proceeds via the following three stages: (1) the system changes from the equilibrium at the initial temperature, 237 °C, to the supercooled disordered spheres at T_{cyl} and T_{sph} within the shortest time covered in this experiment; (2) the system stays at that state for a certain incubation period; (3) after this incubation period, the hexagonally packed cylinders or the spheres with a bcc lattice appear and grow at the expense of the disordered spheres.

To compare the ordering mechanism from the *disordered spheres* with that from the *single-phase state*, the *T*-drop experiment from a temperature above T_{ODT} was performed for Vector 4111/DOP 85.5/14.5. The results indicate that after *T* drop the system first changes from the single-phase state to the disordered spheres within the shortest time covered in this experiment, and the following process is similar to the ordering from the disordered spheres. Thus, it is concluded that the ordering process of Vector 4111 from the *disordered spheres* is identical to that from the single-phase state.

The TEM observation during the ordering revealed that in stage 2, i.e., in the incubation period, the system forms the disordered spheres even in the ordering process of hexagonally packed cylinders. In stage 3 at which I_m is increasing, the ordered grains composed of the cylindrical or spherical microdomains with a long-range order coexist with the disordered spheres. The coexistence of the ordered grains and disordered spheres and the existence of the incubation period suggest that the ordering proceeds via a nucleation and growth process. Furthermore, the TEM observations showed that the shape of the ordered grains composed of the hexagonally packed cylinders is a lenslike oblate ellipsoid in which the cylinders are packed with their axis parallel to the short axis of the oblate ellipsoid and that of the spherical grain is almost directionally independent, i.e., spherical. These results together with the previous result[18] obtained in the ordering process of a symmetric diblock copolymer revealed the shape of the ordered grains in the matrix of the disordered single-phase state or disordered spheres as shown in Figure 16, for lamellar, cylindrical, and spherical microdomains.

Acknowledgment. The authors gratefully acknowledge Prof. C. D. Han for providing the interesting block copolymer sample and collaborating some works (refs 20 and 21), which motivated the present study. This work was supported in part by Research Fellowships of the Japan Society for the Promotion of Science (JSPS) for Young Scientists (6608) and by a Grant-in-Aid for JSPS fellows (00086608) and Scientific Research on Priority Area "Cooperative Phenomenon in Complex Liquids" (07236103) from the Ministry of Education, Science, Sports, and Culture, Japan.

References and Notes

(1) See for example, a review article: Hashimoto, T. *Thermoplastic Elastomers*, 1st ed.; Legge, N. R., Holden, G. R., Schroeder, H. E., Eds.; Hanser: Vienna, **1987**; Chapter 12, Section 3 Hashimoto, T. *Thermoplastic Elastomers*, 2nd ed.; Hanser: Vienna, 1996. Chapter 15A, and references therein.
(2) See, for example, a review article: Bates, F. S.; Fredrickson, G. H. *Annu. Rev. Phys. Chem.* **1990**, *41*, 525 and references therein.
(3) Leibler, L. *Macromolecules* **1980**, *13*, 1602.
(4) Fredrickson, G. H.; Binder, K. *J. Chem. Phys.* **1989**, *91*, 7265.
(5) Hashimoto, T. *Macromolecules* **1987**, *20*, 465.
(6) Harkless, C. R.; Singh, M. A.; Nagler, S. E.; Stephenson, G. B.; Jordan-Sweet, J. L. *Phys. Rev. Lett.* **1990**, *64*, 2285.
(7) Schuler, M.; Stühn, B. *Macromolecules* **1993**, *26*, 112.
(8) Stühn, B.; Vilesov, A.; Zachmann, H. G. *Macromolecules* **1994**, *27*, 3560.
(9) Hashimoto, T.; Sakamoto, N. *Macromolecules* **1995**, *28*, 4779.
(10) Adams, J. L.; Graessley, W. W.; Register, R. A. *Macromolecules* **1996**, *29*, 2929.
(11) Hashimoto, T.; Sakamoto, N.; Koga, T. *Phys. Rev. E* **1996**, *54*, 5832.
(12) Hashimoto, T.; Ogawa, T.; Sakamoto, N.; Ichimiya, M.; Kim, J. K.; Han, C. D. *Polymer* **1998**, *39*, 1573.
(13) Hajduk, D. A.; Tepe, T.; Takenouchi, H.; Tirrell, M.; Bates, F. S. *J. Chem. Phys.* **1998**, *108*, 326.
(14) Rosedale, J. H.; Bates, F. S. *Macromolecules* **1990**, *23*, 2329.
(15) Floudas, G.; Pakula, T.; Fischer, E. W.; Hadiichristidis, N.; Pispas, S. *Acta Polym.* **1994**, *45*, 176.
(16) Floudas, G.; Fytas, G.; Hadichristidis, N.; Pitsikalis, M. *Macromolecules* **1995**, *28*, 2359.
(17) Dai, H. J.; Balsara, B. A.; Garetz, B. A.; Newstein, M. C. *Phys. Rev. Lett.* **1996**, *77*, 3677.
(18) Sakamoto, N.; Hashimoto, T. *Macromolecules* **1998**, *31*, 3292. Sakamoto, N.; Hashimoto, T. *Macromolecules* **1998**, *31*, 3815.
(19) Hohenberg, P. C.; Swift, J. B. *Phys. Rev. E* **1995**, *52*, 1828.
(20) Sakamoto, N.; Hashimoto, T.; Han, C. D.; Kim, D.; Vaidya, N. Y. *Macromolecules* **1997**, *30*, 1621.
(21) Sakamoto, N.; Hashimoto, T.; Han, C. D.; Kim, D.; Vaidya, N. Y. *Macromolecules* **1997**, *30*, 5321.
(22) Hashimoto, T.; Shibayama, M.; Kawai, H. *Macromolecules* **1983**, *16*, 1093.
(23) Fujimura, M.; Hashimoto, T.; Kawai, H. *Mem. Fac. Eng., Kyoto Univ.* **1981**, *43(2)*, 224.
(24) Hashimoto, T.; Suehiro, S.; Shibayama, M.; Saijo, K.; Kawai, H. *Polym. J.* **1981**, *13*, 501.
(25) Suehiro, S.; Saijo, K.; Ohta, Y.; Hashimoto, T.; Kawai, H. *Anal. Chim. Acta* **1986**, *189*, 41.
(26) Fujimura, M.; Hashimoto, H.; Kurahashi, K.; Hashimoto, T.; Kawai, H. *Macromolecules* **1981**, *14*, 1196.
(27) Hendricks, R. W. *J. Appl. Crystallogr.* **1972**, *5*, 315.
(28) Sakamoto, N.; Hashimoto, T., in preparation.
(29) Helfand, E.; Tagami, Y. *J. Chem. Phys.* **1972**, *56*, 3573.
(30) Onuki, A.; Hashimoto, T. *Macromolecules* **1989**, *22*, 879.
(31) Hashimoto, T.; Mori, K. *Macromolecules* **1990**, *23*, 5347.
(32) Percus, J. K.; Yevick, G. *J. Phys. Rev.* **1958**, *110*, 1.
(33) Mastuoka, H.; Tanaka, H.; Hashimoto, T.; Ise, N. *Phys. Rev. B* **1987**, *36*, 1754; **1990**, *41*, 3854.
(34) Kinning, D. J.; Alward, D. B.; Henkee, C. B.; Thomas, E. L. *Macromolecules* **1987**, *20*, 2934.
(35) Shibayama, M.; Hashimoto, T.; Kawai, H. *Macromolecules* **1983**, *16*, 1434.
(36) Hashimoto, T.; Okamoto, S.; Saijo, K.; Kimishima, K.; Kume, T. *Acta Polym.* **1995**, *46*, 463.
(37) In Figure 12c, the diffraction spots corresponding to the first-order scattering maximum exist at different q_m: the spots do not exist on the circle but in the circular band between 0.19 and 0.25 nm^{-1}. This results from the fact that the incident X-ray beam exposed the finite sample area but not infinitesimal area. The scattering from the microdomain structures at the center of the incident beam gave the diffraction spots on the circle at $q = q_m$ with the center at $q = 0$. On the contrary, the scattering from the microdomains on the fringe of the incident beam gave the diffraction spots on the circle at $q = q_m$ with the center at $q \neq 0$. Thus, the diffraction spots of q_m appear to have a distribution in the radial direction. In this experiment, the intensity distribution of the incident beam, i.e., the size of the incident beam on the IP plate, was shown by a Gaussian distribution with a fwhm of 0.056 nm^{-1}, the value of which is consistent with the fact that the scattering maximum exist in the circular band between 0.19 and 0.25 nm^{-1} in Figure 12c.
(38) Koizumi, S.; Hasegawa, H.; Hashimoto, T. *Macromolecules* **1994**, *27*, 6532.
(39) The interfacial tension between the PI block chains anchored to the PS cylinders in the grains and those anchored to the PS spheres in the matrix of the disordered sphere in this work corresponds to the interfacial tension between the PS block chains anchored to the PI cylinders in the grain and HS in the matrix in the mixture of SI and HS.
(40) Wiener, O. *Abh. Math.-Phys. Kl. Saechs. Ges. Wiss.* **1912**, *32*, 507.

MA980411O